Review

Porous silicon biosensors on the advance

Andrew Jane[1], Roman Dronov[1], Alastair Hodges[2] and Nicolas H. Voelcker[1]

[1] School of Chemistry, Physics and Earth Sciences, Flinders University, SA 5001, Australia
[2] Universal Biosensor, Rowville, VIC 3178, Australia

Biosensor research is a rapidly expanding field with an immense market potential spanning a broad spectrum of applications including biomedical diagnostics, environmental monitoring, veterinary and food quality control. Porous silicon (pSi) is a nanostructured material poised to take centre stage in the biosensor development effort. This can be ascribed to the ease and speed of fabrication, remarkable optical and morphological properties of the material (including tuneable pore size and porosity), large internal surface area and the versatile surface chemistry. The past decade has, therefore, seen diverse proof-of-principle studies involving pSi-based optical and electrochemical transducers, which are highlighted here. We also provide comparative analysis of transducer sensitivity, robustness and susceptibility to interferences and cover strategies for sensitivity enhancement by means of signal amplification.

Introduction

A growing need for small, fast, efficient and portable biosensors is reflected by the market value of approximately $11 billion for point-of-care tests in 2005, which is growing at an average rate of 8% per year [1]. The growth of the biosensor market is predicated not only on current and emerging biomedical needs but also on veterinary, food quality and environmental issues. Laboratory and commercial research is attempting to address these needs, often by recruiting emerging and advanced materials with desirable properties for sensing platforms. A case in point is semiconductor silicon, which, since the early days of the semiconductor industry in the 1960s, has provided a platform for development of temperature, pressure and chemical sensors [2–4], in addition to early generation biosensor devices [5–7]. However, it arguably was the discovery of visible light emission from porous silicon (pSi) that sparked a whole raft of research into sensor-related uses for this nanostructured material [8,9]. Some of the favourable properties of pSi, such as its large surface area (up to 800 m^2/g), its fast preparation and its diverse and tuneable optical properties, have certainly predestined this material for sensor applications. Not surprisingly, the past decade has seen a range of successful applications of pSi as a detection platform for biomolecules. The surface area of the material enables for, and is geared to, large amounts of biomolecular interactions occurring over a small working area, thereby facilitating the miniaturization of the sensor. Moreover, being conducive to both optical and electrochemical transducing mechanisms, pSi offers ample opportunities for biosensor design.

pSi is an inorganic material produced during anodic galvanostatic, chemical or photochemical etching of monocrystalline silicon in the presence of hydrofluoric acid (HF). Depending on the etching condition, different nanostructured architectures arise, which usually comprise unidirectionally aligned pores that are perpendicular to the surface, at least in the case of silicon in the (100) crystallographic orientation. The etching solution for anodization usually consists of aqueous HF acting as the etchant and electrolyte and a surfactant or wetting agent such as ethanol to lower the surface tension of the etching solution and permit HF access to the surface. Pore size, porosity and pore depth are adjustable through judicious choice of silicon wafer, dopant and dopant level, current density, HF:surfactant ratio and charge passed [10,11]. Freshly etched pSi is unstable in aqueous medium owing to nucleophilic attacks on the silicon hydride terminated surface by water molecules [12]. Because biosensing experiments are usually conducted in aqueous environments, the pSi surface needs to be stabilized. This is readily achieved by means of oxidation, often in concert with silanization or by hydrosilylation or electrografting [13–15]. Silanization and hydrosilylation also enable the attachment of appropriate biological recognition elements. Given that the surface chemistry of pSi has been covered in a couple of excellent reviews, this topic is not be discussed in this paper [16–18]. The following sections are organized to explore the various ways in which pSi is used as a transducer (the 'heart' of a biosensor), converting specific molecular recognition events into either an optical or electrical signal.

Optical signal transduction

Interference effects in pSi single and double layers

The simplest kind of pSi-based transducer monitors changes in the refractive index that occur in pSi mono- and double-layer films (Box 1) upon a specific bio-recognition event, providing a simple yet effective label-free detection mechanism. The first such pSi biosensor investigated basic biological systems, including DNA hybridization, antibody cascading and the prototypical biotin-streptavidin interaction, using oxidized and silane-functionalized macroporous pSi [19]. These experiments were carried out in a flow cell and used a fibre optics spectrometer. However, early on, conflicting results were obtained. Lin *et al.* [19] observed a blue shift of the fringe

Corresponding author: Voelcker, N.H. (nico.voelcker@flinders.edu.au).

0167-7799/$ – see front matter doi:10.1016/j.tibtech.2008.12.004 Available online 27 February 2009

pattern (i.e. towards shorter wavelengths of the optical spectrum) upon streptavidin binding, which was attributed to a molecular complexation-induced expulsion of charge carriers from the pSi into the bulk silicon, consistent with a reduction in the refractive index. Janshoff *et al.* [13], by contrast, observed the opposite effect: a red shift of the fringe pattern (i.e. towards longer wavelengths) and a corresponding effective optical thickness (EOT) increase. They reasoned and confirmed by theoretical calculation that the phenomenon was due to replacement of water ($n = 1.33$) with protein, which has a higher refractive index ($n \approx 1.42$). The reason for these two contradicting effects has never been conclusively established, but it might be attributed to the different oxidation conditions used in the two papers. With regard to sensitivity, the blue-shift sensor [18] outperformed the red-shift sensor [12] by a factor of 10^5 and achieved detection limits in the sub-picomolar range (Table 1). However, to the best of our knowledge, nobody has been able to reproduce the low detection limits reported in Ref. [19], at least for proteins by means of optical reflectivity on pSi single layers.

A subsequent study established a linear correlation between change in EOT and mass of the introduced protein analyte and also described that nonspecific protein binding in the pores could be suppressed by modification of the porous layer with bovine serum albumin [20]. On the basis of this effect, Schwartz *et al.* [21] implemented a label-free assay of relative antibody-binding affinity to a protein-A-functionalized surface.

Tinsley-Brown *et al.* [22] showed detection of horseradish peroxidase (HRP) by an anti-HRP functionalized pSi layer using a new method for EOT calculation based on orthogonal subspace signal processing algorithms (OSPA). The OSPA approach automatically calibrates the signal via comparison of the sensing reflectivity data to previously gathered reference reflectivity data thereby achieving a reduction in noise and an enhancement in sensitivity. The high accuracy of this technique enabled the monitoring

Box 1. Principles of optical pSi based signal transduction

White light illumination of high-porosity pSi films of several micrometer thickness formed on crystalline silicon results in the reflection from the pSi–medium and the pSi–crystalline silicon interfaces, producing an interference effect called a Fabry–Perot fringe pattern [19] (Figure Ia). This fringe pattern can be detected by a CCD spectrometer (Figure II) and further used to extract characteristics of the pSi layer, such as its refractive index and its thickness. The maxima in the fringe pattern occur at λ_m and are related to the physical properties of the pSi via:

$$m = \frac{2nd}{\lambda_m}$$

where m refers to the fringe order, d the film thickness and n the average refractive index of the layer at wavelength λ_m. Plotted as a function of wavelength ($1/\lambda$), the maxima are equally spaced because the refractive index is approximately independent of wavelength. Fourier transformation of the reflectance spectra provides intensity versus frequency (nm^{-1}) information, affording a peak proportional to the effective optical thickness (EOT) of the film (EOT = nd) [19,21,59].

A change in the refractive index of the porous layer (e.g. upon binding of biological macromolecules) manifests itself in a shift of the fringe pattern and a corresponding change in EOT (Figure II).

By varying the current density during etching process, pSi can assume double- or multilayered structures [37,60] (Figure Ib,c). Alternating between two distinct currents in real time in a stepwise manner results in Bragg reflectors where the porous film displays a corresponding discrete modulation in porosity and, hence, in refractive index with depth [61,62]. When the Bragg condition for a photonic crystal is met, light at a defined wavelength corresponding to the photonic bandgap of the crystal is reflected, while the remaining light is absorbed (Figure Ic). Microcavities are 1D photonic bandgap structures that include a spacer layer positioned between two Bragg reflectors [61,63] (Figure Id). This results in the formation of a narrow photonic resonance, which appears as a dip in the reflectance spectrum and is highly sensitive to changes in refractive index such as those arising from binding of biomolecules in the pores.

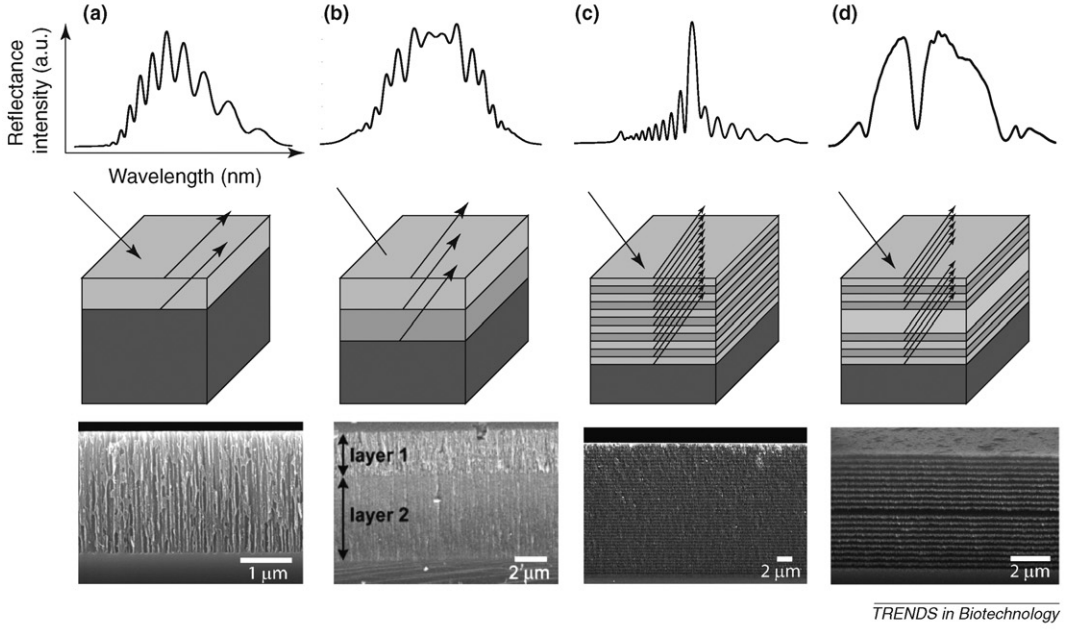

Figure I. Different pSi structures and their corresponding reflectance spectra. **(a)** Single layer; **(b)** double-layer [23]; **(c)** multilayer [64]; and **(d)** microcavity [49]. Abbreviations: a.u., arbitrary units.

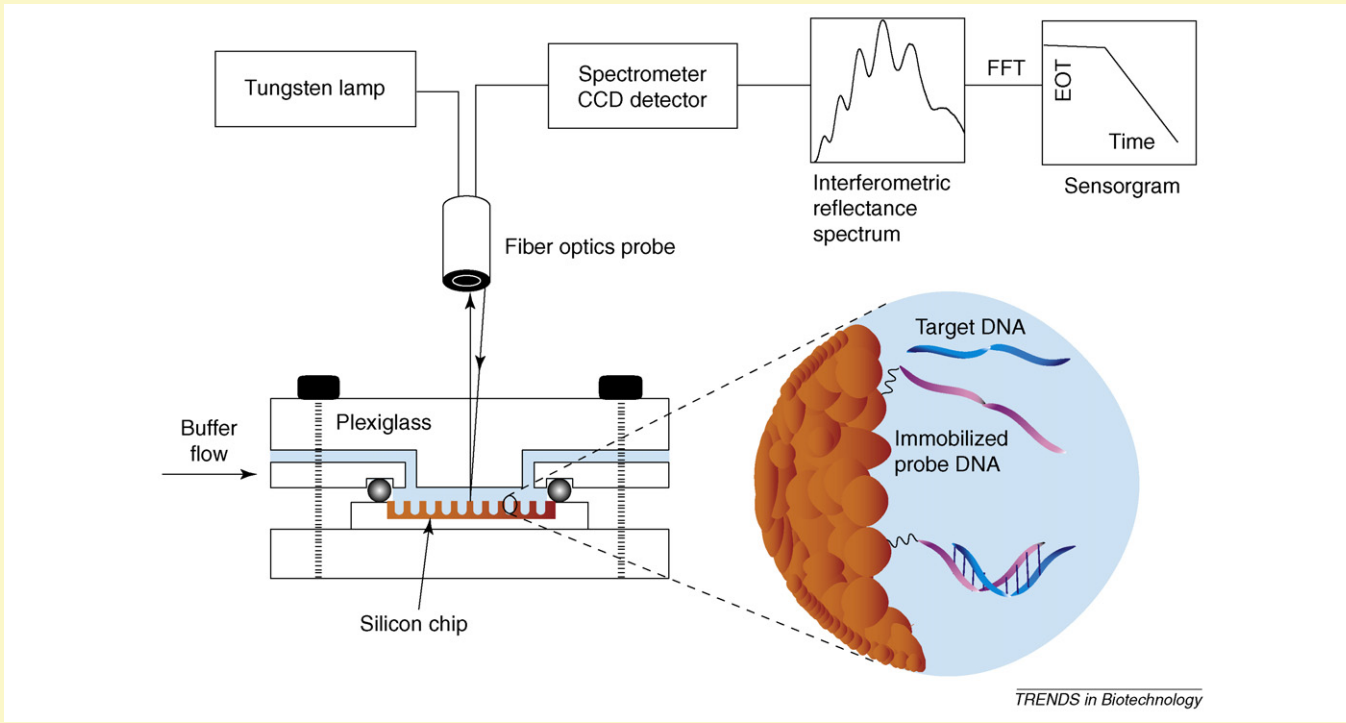

Figure II. Experimental set-up used in most pSi biosensors based on optical reflectivity. The pSi surface is illuminated with white light from a bifurcated fibre optic cable. Reflected light is captured by fibre optics and detected with a charge couple device (CCD). The obtained reflectance spectrum is Fourier transformed (FFT) into an effective optical thickness (EOT), which is monitored over time (sensorgram). The zoom-in shows an example for a bio-recognition event, here DNA hybridization between immobilized probe DNA and target DNA in solution, that occurs within the pSi layer. Such events within the layer are manifested as changes in the reflectivity spectra, which can be quantified forming the basis of pSi optical detection.

of changes in the refractive index up to 10 ppm and the detection of only 100 pg/mm^2 of protein.

Drift of the EOT signal and the effect of changing and complex matrices (e.g. body fluids) often interfere with biosensor operation and hamper its performance. An interferometric biosensor featuring two stacked pSi layers of different pore size was fabricated by Pacholski *et al.* [23] in an attempt to address these issues. Here, an architecture that comprises an outer layer made up by larger pores and an inner layer with smaller pores permits the simultaneous separation and detection of biomolecules based on size exclusion effects. The inner layer effectively serves as a reference layer. Reflectance spectra obtained from these double-layer sensors contain three superimposed interference patterns that provide independent information of the binding, adsorption or partitioning events that occur in these layers. This concept was demonstrated using bovine serum albumin (BSA) and sucrose as the

Table 1. Comparison of the performance of different pSi-based biosensors[a]

Transducer	Analyte	Concentration or concentration range	Sensitivity for analyte	Detection limit	Refs
Single pSi layer	DNA	10^{-15}–10^{-6} M	$\sim10^{12}$ nm × L/mol	9×10^{-15} g/mm^2	[19]
	Biotin	10^{-5} M	n/d	n/d	[30]
	Streptavidin	10^{-12}–10^{-5} M	n/d	5.5×10^{-14} g/mm^2	[32]
	Antibody	10^{-12} M	n/d	n/d	[19]
		10^{-6} M	n/d	$1–10 \times 10^{-9}$ g/mm^2	[13]
		$1.25–5 \times 10^{-7}$ g/mL	n/d	n/d	[33]
Rugate filter	Subtilisin	10^{-8}–10^{-6} M	n/d	n/d	[41]
	Pepsin	$7–14 \times 10^{-6}$ M	~1 L/(min × g)	n/d	[40]
Microcavity	Glutathione-*S*-transferase	$1–40 \times 10^{-6}$ M	n/d	5×10^{-11} g/mm^2	[49]
	Antibody	$2–10 \times 10^{-3}$ g/mL	0.325 nm × L/g	n/d	[53]
	Intimin-ECD	$4–15 \times 10^{-6}$ M	3×10^5 nm × L/mol	n/d	[54]
Electrochemical (impedance)	DNA	$>10^{-7}$ M	n/d	n/d	[55]
Electrochemical (amperometry)	Cholesterol	$1–50 \times 10^{-3}$ M	0.2656×10^{-3} A × L/mol	n/d	[56]
	Bilirubin	$2–20 \times 10^{-6}$ M	0.15354 A × L/mol	n/d	[56]
	Alanine aminotransferase	1.3–250 U/L	0.13698×10^{-6} A × L/U	n/d	[56]
	Aspartate aminotransferase	1.3–250 U/L	0.45439×0^{-6} A × L/U	n/d	[56]

[a]n/d, not determined.

macromolecular analyte and the small probe molecule, respectively, and measured molecule penetration into a macroporous (50–100 nm) top layer accessible to both BSA and sucrose and a mesoporous (<20 nm) underlying layer only accessible to sucrose.

Photoluminescence-based transduction

Photoluminescence (i.e. emission of secondary photons upon photoexcitation) of pSi has been harnessed for sensing applications ever since room temperature photoluminescence has been discovered in the early 1990s [9]. A large number of different chemosensors have been implemented based on photoluminescence, including sensors for organic solvents, explosives and hazardous waste [24–28]. This signal-transduction method has also been adopted for biomolecular recognition. For example, detection of immunocomplex formation has resulted in photoluminescence quenching [29]. More recently, Di Francia *et al.* [30] found evidence for label-free transduction of DNA hybridization. In these cases, photoluminescence quenching was attributed to non-radiative recombination processes. There is a conspicuous gap in the literature with respect to detection of biomolecules based on pSi photoluminescence effects. This could be due to the fact that measuring changes in photoluminescence is associated with a greater error compared with measuring wavelength shifts. In addition, signal transduction by photoluminescence seems to be particularly vulnerable to interferences in the sample matrix because photoluminescence of pSi is known to be affected by a range of molecular species and through several different mechanisms, including non-radiative recombination of excitons, electron transfer and interfacial charging [8,10,24–27,31].

Increasing sensitivity through signal amplification

The remarkable sensitivity obtained by Lin *et al.* [19] certainly invited exploration of the concept of binding-signal amplification. But, although the phenomenon of charge-carrier mobilization induced by biomolecular complexation as described in Ref. [19] has not been demonstrated successfully again, the idea of triggering profound changes in refractive index upon oxidation or corrosion of pSi induced by target-molecule recognition has been pursued in more recent studies [32–34]. Corrosion of a pSi layer results in a profound, albeit irreversible, change to porosity, pore size and, hence, refractive index of the porous layer and might, therefore, potentially lead to improvements in sensitivity compared with the red-shift sensors, such as the one described in Ref. [13].

Steinem *et al.* [32] showed that recognition of complementary (c)DNA oligonucleotides on the surface of oxidized pSi can result in the enhanced corrosion of pSi made from p-type silicon (Figure 1b,c). The authors postulated that the corrosion of the pores was the result of enhanced oxidation and corrosion of the pSi that occurred in the presence of rigid and highly negatively charged double-stranded DNA. According to this proposed mechanism, the change in the electrostatic field upon hybridization attracted positive holes to the pSi–buffer interface, thereby facilitating nucleophilic attack of water molecules and subsequent oxidation and dissolution of silicon. Consistent

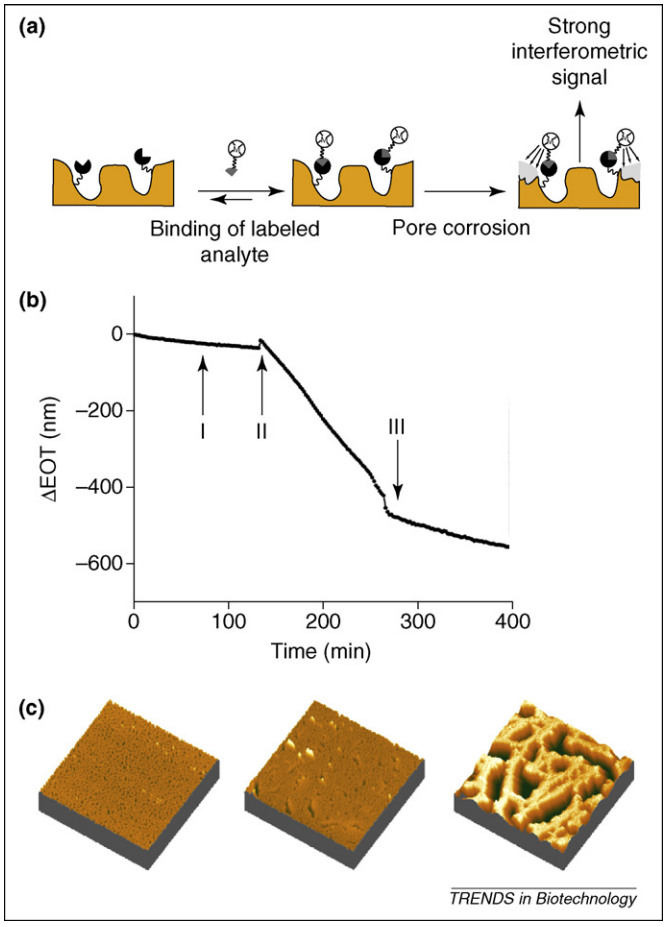

Figure 1. Biomolecule detection via corrosion of the pSi surface. **(a)** Schematic illustration showing an optical transducer design based on the catalysis of oxidative corrosion of a pSi layer induced by a transition metal catalyst. Adapted, with permission, from Ref. [34]. **(b)** Sensorgram (EOT change over time) for DNA detection. An EOT baseline was obtained in PBS. At time point (I) non-cDNA was added. At time point (II) cDNA was added, and at time point (III) a buffer wash was applied. **(c)** This panel shows atomic force microscopy images (14 ξ 14 μm^2) that were taken (from left to right) before addition of cDNA, after 1 h and after 2 h of incubation with cDNA. Corrosion is evident from enlargement of the pores. Reproduced, with permission, from Ref. [32].

with this hypothesis, the rate of corrosion increased with doping level of the p-type silicon. Importantly, the corrosion effect was absent upon addition of Mg^{2+} cations or charge neutral peptide nucleic acids (PNA), confirming that the corrosion was indeed caused by the negative charge of the DNA. This corrosion phenomenon was akin to a signal amplification enabling detection of DNA in concentrations as low as 0.1 amol/mm^2 and effectively demonstrated the ultrasensitivity that could be achieved by pSi-based transducers.

Building upon this work, Voelcker *et al.* [34] showed that molecules other than double-stranded DNA are capable of inducing the corrosion of inorganic pSi and of generating strong interferometric signals. For example, certain transition metal complexes, such as nickel(II)cyclam, were identified in a screen to be potent catalysts of ozone-oxidized pSi corrosion [34] (Figure 1a). This concept was exploited in the design of a transducer for ligand–receptor recognition. Using a nickel(II)cyclam derivative as a catalytic label, DNA hybridization and avidin-biotin binding events could be detected in submicromolar quantities

owing to their ability to induce an increased rate of pSi corrosion. The Voelcker group has also recently demonstrated that horseradish peroxidase, an enzyme commonly used as a label for antibodies, induces the corrosion of pSi in the presence of a suitable substrate [33] (Szili, E.J. *et al.*, unpublished) and gives rise to indirect enzymatic degradation of pSi. The product of the enzymatic reaction is a radical cation, which induces oxidative hydrolysis of the surface. The resulting distinct interferometric read-out, which, for example, enabled the detection of antibodies in amounts as lows as 125 ng/mL, was localized on the solid surface rather than in solution, in conspicuous contrast to a traditional enzyme-linked immunosorbent assay (ELISA). The surface-bound signal generated in the pSi biosensor both permits multiplexing by means of a microarray and offers avenues for miniaturization. Although these sensors [33,34] require labelling of the analyte or operation as a competitive assay, they offer the advantage of being applicable to most biomolecular analytes.

1D photonic crystals

As discussed before, pSi is often fabricated in the form of a single layer of a certain thickness. However, by periodically changing the current density, so-called 1D photonic crystals can be generated. These architectures include Bragg reflectors and microcavities that are produced by alteration of the etching current in a stepwise manner (Box 1) and rugate filters, which are obtained by the sinusoidal variation of the current density. Rugate structures offer cleaner reflectance spectra because unwanted sidelobes are suppressed; however, on the downside, their peak reflectance is reduced [35,36]. By modifying the thickness and refractive index contrast of the layers, the resulting reflectance features across the optical spectrum can be tailored for sensing purposes in a similar manner to single-layer pSi. In addition, several current waveforms can also be overlaid to produce even more complex optical structures such as superlattices that result in spectral barcodes [37,38].

The sensitivity of various pSi architectures with regard to changes in the refractive index of a liquid has been investigated by Anderson *et al.* [39]. A decrease in reflectivity at a fixed wavelength from a single layer, Bragg reflector and microcavity upon introduction of 0.05–1.0 wt% sucrose solution was analyzed and compared with the theoretically predicted values. The authors experimentally showed that the Bragg reflector provided the highest decrease in reflectivity upon addition of sucrose, although the theoretical estimation indicated that the microcavity should exhibit a larger response. Two recent studies used pSi rugate filters in combination with proteases [40,41]. These studies enable the evaluation of protease activity and the detection of its protein substrates via the detection of the produced peptide fragments. Orosco *et al.* [40] produced a pSi multilayer film that had been hydrophobized by methylation of the micropores, which restricted the entry of large biomolecules. The protein zein was adsorbed on the top surface of the porous film, and the underlying pores remained air-filled. Incubation with proteases, in this instance with pepsin, led to zein digestion and subsequent infiltration of the small peptide fragments and water into the vacant pores (Figure 2). The pore loading caused an increase in the refractive index of the pSi layer, which, in turn, induced a measurable red shift to the reflectance band. With this sensor, protease concentrations as low as 7 μM could be detected, whereas at protease concentrations higher than 14 μM the changes to the porous matrix were so profound that they could be observed with the naked eye.

An alternative method of protease detection involved the covalent immobilization of peptides acting as protease substrates within a macroporous structure that enabled the diffusion of biomolecules through the pores. Kilian *et al.* [41] exposed the peptide-modified photonic crystal to the protease subtilisin, which resulted in peptide cleavage. The generated amino acid fragments were removed from the porous layer, thereby reducing its refractive index. When the reflectance spectrum was measured in air, a blue shift of the photonic resonance was observed owing to the decrease of the refractive index. In comparison with the biosensor reported by Orosco *et al.* [40], this device was able to detect considerably lower protease concentrations of 37 nM (Table 1).

Biosensors adapted to cell and tissue culture situations have substantial potential to underpin and to enable discoveries in emerging areas of biotechnology including high-throughput drug testing, proteomics and stem-cell technologies. Sailor *et al.* [42,43] have developed the concept of a so-called 'smart Petri dish', which enables monitoring of the health of prokaryotic and eukaryotic cell cultures by

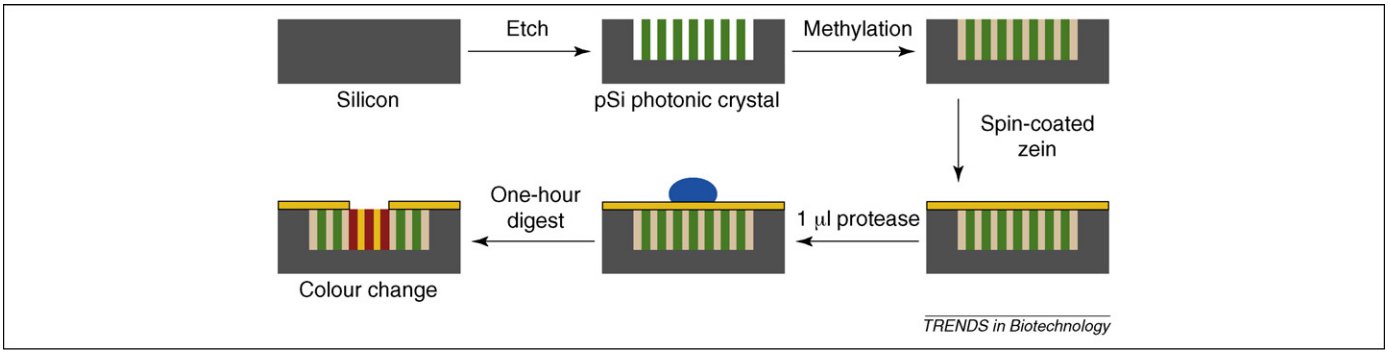

Figure 2. Schematic illustration of an assay for pepsin activity. The pSi sample is first methylated to achieve a hydrophobic interface. It is then spin coated with the protein zein, which is excluded from the porous layer of the photonic crystal. Addition of a protease subsequently results in the digestion of this protein, and proteolytic peptide fragments are able to infiltrate the photonic crystal and lead to a change of refractive index of the porous multilayer, which in turn gives rise to a red shift of the photonic response and a macroscopic colour change. Adapted, with permission, from Ref. [40].

means of light scattering from the surface of a rugate filter. The surface of a pSi rugate filter is illuminated with white light at an oblique angle, and a charge-coupled device (CCD) spectrometer was positioned perpendicular to the surface. Specular reflectance from the photonic reflectance band cannot be observed in this configuration. However, introduction of a scattering centre on the rugate filter surface, such as a biological cell, resulted in the scattering of light emanating from the surface, which can be detected by the spectrometer.

This format was used to monitor physiological changes occurring in primary rat hepatocytes that affected their viability [42]. The rugate filter was coated with polystyrene, which was rendered hydrophilic and conducive to cell adhesion by oxygen plasma treatment. A monolayer of hepatocytes seeded onto the surface was exposed to the toxins cadmium chloride and acetaminophen to induce either direct or metabolite-induced cell death. Morphological changes and, in particular, cell death resulted in an increase in the amount of light scattering and light from the photonic resonance being captured by the CCD spectrometer, which was attributed to changes in mitochondrial composition and lipid-droplet formation upon or immediately before cell death (Figure 3). Using the CCD spectrometer, the study reported an increase in light scattering and, thus, the occurrence of cell damage within approximately two hours of addition of 50 μM Cd^{2+} to cell-culture medium; this is several hours earlier than any change in cell viability could be detected by a conventional tetrazolium salt cell-viability assay or a live/dead staining assay. Importantly, previous cell-growth studies on pSi had established that the tetrazolium salt assay provided a false positive signal in the presence of pSi, which acts as a reducing agent [44]. The authors avoided

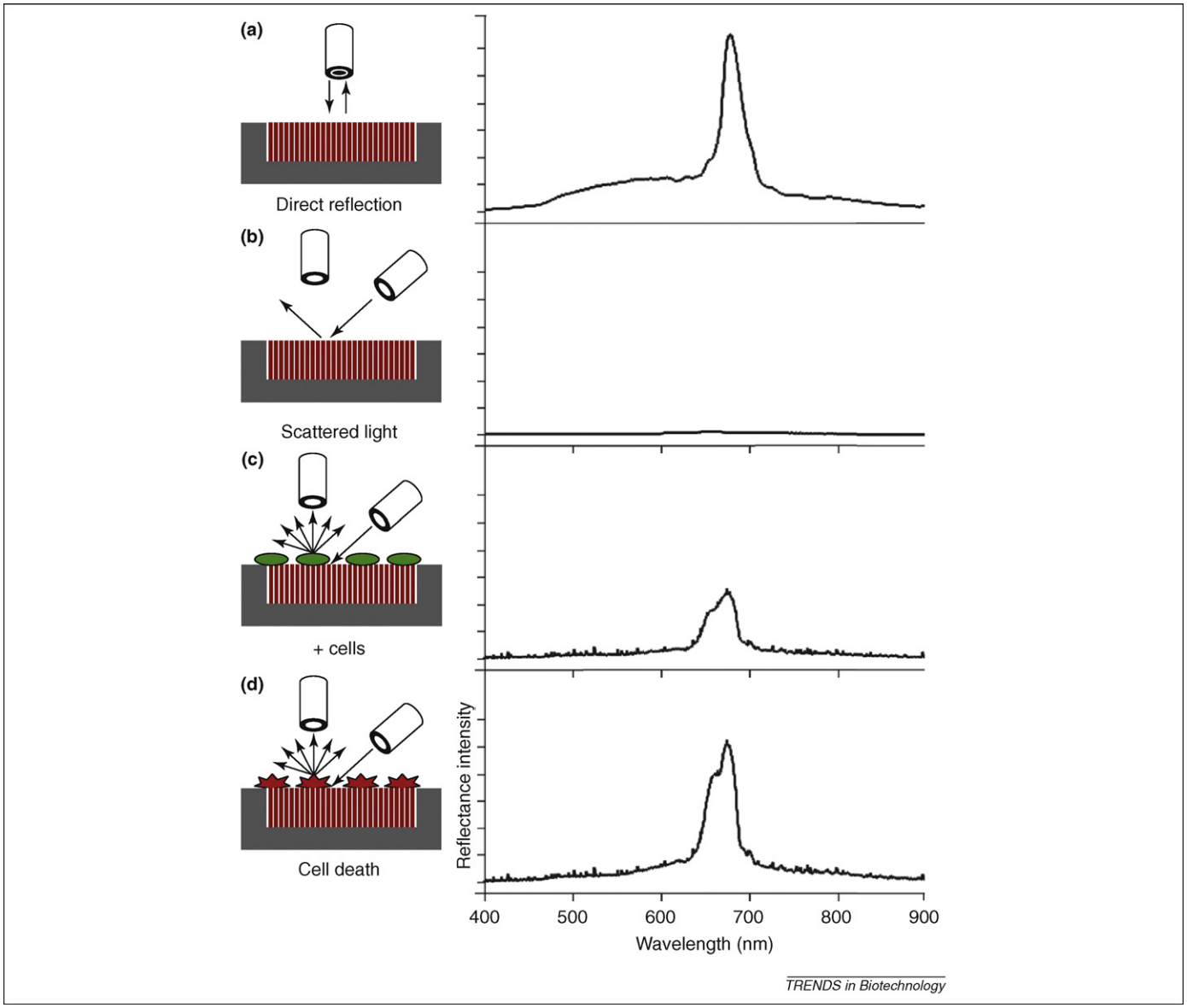

Figure 3. Schematic illustration of a smart Petri dish. **(a)** Photonic resonances generated by a light source normal to the surface are detected by the CCD detector positioned on axis. **(b)** Resonances generated by an off-normal light source are not detected by the CCD normal to the surface. **(c)** Seeding cells on the smart Petri dish introduces scattering centres that divert some of the light into the CCD, which can be detected as a peak in the resulting spectrum. **(d)** Changes in cell morphology, for instance as a result of reduced cell viability or cell death, alter the scattering efficiency of the cells, which can be detected as changes in peak intensity. The increased scattering effect that occurs upon cell death originates from changes in the mitochondrial composition and lipid droplet formation. Adapted, with permission, from Ref. [42].

this artefact by coating the pSi layer with polystyrene. A control sample that was not exposed to Cd^{2+} did not exhibit any large changes in light intensity over the same time period; this eliminated cell division as a contributing factor to scattering intensity. A considerable advantage of the smart Petri dish format is that cell morphological changes can also be visualized by conventional light microscopy in reflection mode. Although this approach is clearly more sensitive to early cytotoxicity, quantitative cell-viability measurements have not yet been reported because the scattering intensity reached a plateau before cell viability was lost completely. It is worth pointing out that because the smart Petri dish does not require any tampering with cells, such as sampling of media or the addition of dyes for cells staining, it provides excellent scope for a non-intrusive and real-time monitoring of cell behaviour.

More recently, Alvarez *et al.* [43] adapted the smart Petri dish concept to a simple device for monitoring in real time the growth of *Pseudomonas syringae* bacteria and their lysis upon viral infection. The authors could establish a linear relationship between the number of bacteria and scattering intensity with a detection limit that was comparable to current spectrometer-based turbidity systems. Bacterial cell lysis induced by phage virus infection and replication resulted in a dramatic decrease in light intensity owing to the removal of the scattering centres.

It is worth highlighting the potential of incorporating recognition elements into the porous layer that would enable monitoring of specific cellular byproducts or combining biosensing with the delivery of bioactive molecules from the high porous volume of the pSi. Such 'fit-for-purpose' and multifunctional devices are poised to become the next-generation tissue-culture materials.

Multilayered pSi offers the additional advantage of being versatile in that pSi films can be processed into microparticles using sonication [38], which maintains their photonic resonances. Given the tuneable and responsive optical signatures that can be programmed into these particles, the term 'smart dust' might seem fitting. Superimposing several sinusoidal current waveforms produces a series of reflectance peaks with positions and intensities defined by the applied waveform. This characteristic gives rise to a large combinatorial space, such that the reflectance spectrum from a particle can be used as an encoding mechanism to, among other things, identify captured biomolecules from the reflectance peak of the particle to which they are attached. Cunin *et al.* [45] provided the proof of principle for this approach by being able to distinguish between rat and bovine albumin using microparticles encoded with a spectral barcode. The ease with which the pSi particles can be encoded and manufactured, coupled with the biocompatibility and degradability of the material, provide significant advantages over other coding systems, such as those employing potentially toxic CdSe nanoparticles [46,47].

pSi microcavities

Chan *et al.* [48] fabricated a biosensor capable of differentiating between Gram-negative and Gram-positive bacteria that utilized red shifts to the resonance peaks of a pSi microcavity (Box 1). The receptor *ter*-cyclo pentane (TWTCP), which recognizes 'lipid A', a lipopolysaccharide specific to Gram-negative bacteria, was immobilized in the pores. Thus, this generated sensor was able to detect lipid A with a detection limit of ~1.7 μg. However, a comparison with other methods used to distinguish Gram-positive and Gram-negative bacteria is difficult because the detection limit is typically reported as colony forming units (CFU) rather than as a bacterial mass.

A recent comprehensive study of DeLouise *et al.* [49] aimed at establishing the optical detection limit for mesoporous pSi microcavities using the enzyme glutathione-*S*-transferase as a probe. Wavelength shift sensitivities in the order of 500 nm per refractive index unit (RIU) were observed. Although this value is lower than for surface plasmon resonance sensors, the microcavity sensor with its high surface area could potentially offer other advantages, in particular for the detection of analytes with relatively weak affinity [50–52]. The detection limit achieved with this system was an impressive 50 pg/mm^2. The work also afforded a fundamental understanding of the dependence of microcavity response to refractive index changes on certain parameters, such as device architecture and morphology. Sensitivity is deemed to be independent of the thickness of the device, the thickness of the spacer layer and the Q factor of the device, which is defined as $Q = \lambda/\Delta\lambda$, where λ is a resonance wavelength and $\Delta\lambda$ is the full width at half maximum (FWHM) of the resonance peak. The initial resonance wavelength seemed to be the only parameter on which the bulk RIU sensitivity strongly depended.

Bonanno *et al.* [53] recently reported the fabrication of a label-free optical biosensor for the detection of rabbit IgG in whole blood using a pSi microcavity. Leveraging size-exclusion filtering capabilities, the device was able to detect antibodies in either undiluted serum or even whole blood (Figure 4) via a wavelength shift. Biotin-streptavidin chemistry was used to immobilize the antibody on the pSi surface. High target binding specificity, minimal cross-reactivity and a linear detection range of 2–10 mg/mL was established.

Ouyang *et al.* [54] developed a microcavity sensor that operated by analyzing the induced red-shift in the absorbance peak that is caused by the binding of an analyte to an immobilized probe molecule. The device was targeted at the detection of an extracellular domain of intimin (intimin-ECB), a protein associated with the pathogenicity of enteropathogenic *Escherichia coli*. Tir–IBD, the translocated intimin receptor–intimin binding domain, acted as the probe and has been covalently immobilized to the surface of the pSi. After optimising the concentration of probe molecules, intimin-ECB could be detected in a concentration of 4 μM. Exposure of the sensor to cell lysate from an *E. coli* BL21 cell line, which expresses intimin-ECD, resulted in a distinct red shift owing to selective target recognition among the entirety of bacterial proteins, whereas lysate from control bacteria not expressing the protein did not give a wavelength shift.

Electrochemical transduction with pSi

Perhaps somewhat surprisingly, electrochemical transducers have been in the shadow of optical sensors, at least as

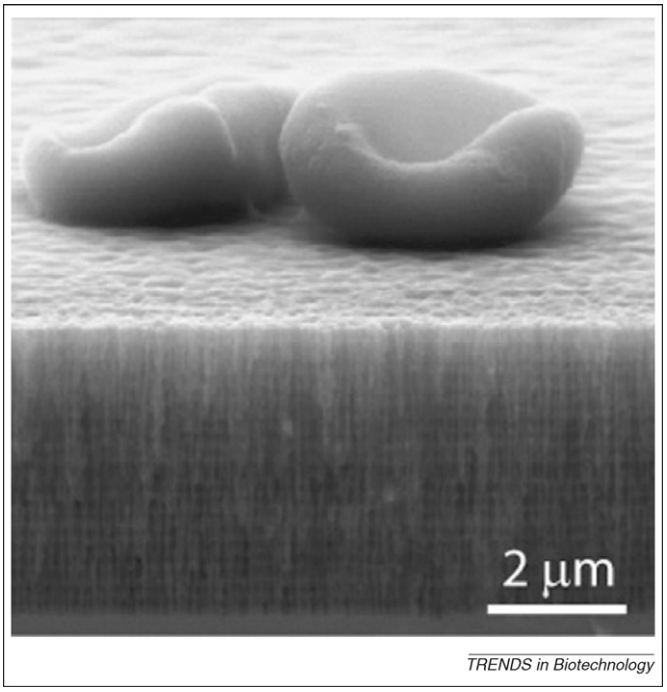

Figure 4. Cross section of a pSi microcavity biosensor. This scanning electron micrograph (SEM) image demonstrates the size-exclusion filtering effects of the pSi pores where blood cells are excluded from entering into the sensing layer. Reproduced, with permission, from Ref. [53].

far as pSi is concerned. Yet, there are several recent and promising reports that are worthwhile summarizing (Table 1). For instance, exploitation of the semiconductor properties of pSi has produced biosensors that operate by modulating the space-charge region in the crystalline silicon columns and the dielectric constant of the porous layers upon binding of charged molecules [55]. Macroporous pSi, containing pore diameters of 1–2 μm, was functionalized with poly-L-lysine before the probe DNA was immobilized via electrostatic interactions. Upon introduction of a solution containing the cDNA, hybridization was detected via a reduction in pSi impedance and afforded a detection limit in the region of 100 nM. The crucial requirement of a charged target molecule was confirmed by a neutral PNA control, which did not give rise to an impedance change.

Traditionally, electrochemical transduction involves the conversion of an electro-active substance in the presence of the target analyte. The incorporation of pSi into such devices offers the advantage of a substantially larger sensing area compared with flat electrodes. Song *et al.* [56] adhered pSi to a platinum working electrode to greatly increase the effective surface area of the electrode and were able to achieve a high sensitivity and selectivity for liver disease markers such as cholesterol, bilirubin, alanine aminotransferase and aspartate aminotransferase. Another example, the amperometric biosensor, which consists of an array of four pSi working electrodes functionalized with different analyte-selective enzymes and separated by a polydimethylsiloxane (PDMS) microfluidic structure, was shown to be capable of detecting four different markers in parallel. The enzymatic reactions produced H_2O_2 upon conversion of their respective analytes, which then underwent electro-oxidation and resulted in anodic current that was proportional to the analyte concentration [57].

Setzu *et al.* [58] developed a potentiometric biosensor for the detection of tryglycerides for metabolomics and food analysis. In this setup, lipase enzyme was immobilized within the pSi layer and induced hydrolysis of a triglyceride such as tributyrin. Hydrolysis resulted in a decrease of the pH, which in turn shifted the open circuit potential. Another advantage of this approach was that the immobilization of the enzyme within pSi layer considerably increased the working life of the sensor compared with other lipase-based triglyceride-detection methods.

Conclusions and outlook

pSi as a platform material for biosensors has engendered several high-impact proof-of-principle studies in this field. These include studies on optical transducers based on reflective interference, photonic resonance or photoluminescence effects, in addition to electrochemical transducers. Although in some instances a highly sensitive detection of biomolecules of femtomolar concentrations could be demonstrated, other transducers described here are currently less sensitive than the conventional ELISA assay when concentration is the determining factor. However, these sensors clearly outperform ELISA assays in terms of other important characteristics such as response time, minimum volume requirements and, in many cases, label-free operation. Furthermore, the described optical signal transduction is inherently affordable and requires only inexpensive device components such as a white light source and a CCD spectrometer. Fabrication of pSi is compatible with an array format required for high-throughput systems and pSi sensors are, therefore, conducive to multiplexing. Lastly, miniaturization of a pSi sensor can be easily achieved by combining well-established silicon microfabrication methods with pSi formation.

We expect that further developments in patterning and miniaturization will open a path to the development of small, highly parallel pSi-based biochips for the simultaneous detection of multiple analytes, and the biocompatibility of pSi might enable the design of implantable biosensors that are able to monitor biological systems in real time and *in vivo*.

Several challenges will need to be overcome to be able to make biosensors based on pSi a practical reality as a commercial product. They fall into two main areas: those concerning the fabrication of pSi into cost effective and robust devices, and those addressing the ability to handle real-world sample matrices such as whole blood.

pSi is a relatively expensive sensing material compared with, for example, carbon ink that is used in some electrochemical glucose sensors or porous polymer membranes used in lateral flow devices. Therefore, to be cost effective relatively small areas of thin silicon wafer need to be used. This presents a handling and fabrication challenge in how to machine assemble fragile components into test devices. Other challenges to achieving cost-effective device fabrication include the safe handling of materials, such as the HF needed to etch the silicon.

Regarding medical applications, two potential markets are central pathology laboratory testing and point-of-care testing, in which the test is performed close to the patient [1]. Central laboratory tests will typically have to handle blood plasma samples and point-of-care tests will have to handle whole blood. Whole blood, in particular, presents challenges because it is subject to a range of potential interferences from the presence of the red cells and species that chemically interfere. In addition to the colour of the red cells potentially interfering optically, differences in the volume fraction of red cells in a blood sample can interfere with the concentration determination and typically needs to be compensated for. pSi shows some promise in terms of whole-blood analysis because size exclusion in the porous layer can be exploited [53] and because measurements of optical changes (e.g in EOT or in peak wavelength) occurring over time could be used to enable such interferences [34].

The future will show whether pSi biosensors will succeed in escaping the laboratory and conquer a market share among other devices for pathology laboratory texting, point-of-care diagnostics and environmental monitoring, or provide additional and valuable tools for the fundamental study of the kinetics and thermodynamics of ligand–receptor interactions.

References

1 [No authors listed] (2006) *The Worldwide Market for in vitro Diagnostic Tests*, Kalorama Information
2 Fruett, F. and Meijer, G.C.M. (2003) . In *The Piezojunction Effect in Silicon Integrated Circuits and Sensors (The Kluwer International Series in Engineering and Computer Science)* (Ismail, M., ed.), Springer
3 Zimmermann, H. (2004) . In *Silicon Optoelectronic Integrated Circuits (Springer Series in Advanced Microelectronics)* (Itoh, K. *et al.*, eds), Springer
4 Chaniotakis, N. and Sofikiti, N. (2008) Novel semiconductor materials for the development of chemical sensors and biosensors: a review. *Anal. Chim. Acta* 615, 1–9
5 Parce, J.W. (1989) Detection of cell-affecting agents with a silicon biosensor. *Science* 246, 243–247
6 Bataillard, P. *et al.* (1993) An integrated silicon thermopile as biosensor for the thermal monitoring of glucose, urea and penicillin. *Biosens. Bioelectron.* 8, 89–98
7 Madou, M. and Tierney, M.J. (1993) Required technology breakthroughs to assume widely accepted biosensors. *Appl. Biochem. Biotechnol.* 41, 109
8 Canham, L.T. and Cullis, A.G. (1991) Visible light emission due to quantum size effects in highly porous crystalline silicon. *Nature* 353, 335–338
9 Canham, L.T. (1990) Silicon quantum wire array fabrication by electrochemical and chemical dissolution. *Appl. Phys. Lett.* 57, 1046
10 Canham, L.T. (1997) *Properties of Porous Silicon.* (1st edn), The Institute of Electrical Engineers
11 Föll, H. *et al.* (2002) Formation and application of porous silicon. *Mater. Sci. Eng.* 39, 93–141
12 Allongue, P. (1993) Etching of silicon in NaOH solutions: electrochemical studies of n-Si(111) and n-Si(100) and the mechanism of the dissolution. *J. Electrochem. Soc.* 140, 1018–1026
13 Janshoff, A. *et al.* (1998) Macroporous p-type silicon fabry-perot layers. Fabrication, characterization, and applications in biosensing. *J. Am. Chem. Soc.* 120, 12108–12116
14 Buriak, J.M. *et al.* (1999) Lewis acid mediated hydrosilylation on porous silicon surfaces. *J. Am. Chem. Soc.* 121, 11491–11502
15 Robins, E.G. *et al.* (1999) Anodic and cathodic electrografting of alkynes on porous silicon. *Chem. Commun. (Camb.)* 2479–2480
16 Buriak, J.M. (2002) Organometallic chemistry on silicon and germanium surfaces. *Chem. Rev.* 102, 1271–1308
17 Schmeltzer, J.M. and Buriak, J.M. (2004) Recent developments in the chemistry and chemial applications of porous silicon. In *The Chemistry of Nanomaterials: Synthesis, Properties and Applications* (Rao, C.N.R. *et al.*, eds), pp. 518–550, Wiley-VC
18 Salonen, J. and Lehto, V-P. (2008) Fabrication and chemical surface modification of mesoporous silicon for biomedical applications. *Chem. Eng. J.* 137, 162–172
19 Lin, VS-Y. *et al.* (1997) A porous silicon-based optical interferometric biosensor. *Science* 278, 840–843
20 Dancil, K.P. *et al.* (1999) A porous silicon optical biosensor: detection of reversible binding of IgG to a ptotein A-modified surface. *J. Am. Chem. Soc.* 121, 7925–7930
21 Schwartz, M.P. *et al.* (2007) Using an oxidized porous silicon interferometer for determination of relative protein binding affinity through non-covalent capture probe immobilization. *Phys. Status Solidi, A Appl. Res.* 204, 1444
22 Tinsley-Bown, A. *et al.* (2005) Immunoassays in a porous silicon interferometric biosensor combined with sensitive signal processing. *Phys. Status Solidi, A Appl. Res.* 202, 1347–1356
23 Pacholski, C. *et al.* (2005) Biosensing using porous silicon double-layer interferometers: reflective interferometric Fourier transform spectroscopy. *J. Am. Chem. Soc.* 127, 11636–11645
24 Jin, W.J. *et al.* (1998) Organic solvent induced quenching of porous silicon photoluminescence. *Spectrochim. Acta A Mol. Biomol. Spectrosc.* 54, 1407–1414
25 Content, S. *et al.* (2000) Detection of nitrobenzene, DNT, and TNT vapors by quenching of porous silicon photoluminescence. *Chem. Eur. J.* 6, 2205–2213
26 Chvojka, T. *et al.* (2004) Mechanisms of photoluminescence sensor response of porous silicon for organic species in gas and liquid phases. *Sens. Actuators B Chem.* 100, 246–249
27 Mahmoudi, B. *et al.* (2007) Photoluminescence response of gas sensor based on CHx/porous silicon – effect of annealing treatment. *Materials Science & Engineering. B. Solid-State Materials for Advanced Technology* 138, 293–297
28 Yin, F. *et al.* (1998) Photoluminescence enhancement of porous silicon by organic cyano compounds. *J. Phys. Chem. B* 102, 7978–7982
29 Starodub, V.M. *et al.* (1999) Control of myoglobin level in a solution by an immune sensor based on the photoluminescence of porous silicon. *Sens. Actuators B Chem.* 58, 409–414
30 Francia, G.D. *et al.* (2005) Towards a label-free optical porous silicon DNA sensor. *Biosens. Bioelectron.* 21, 661–665
31 Stewart, M.P. and Buriak, J.M. (2000) Chemical and biological applications of porous silicon technology. *Adv. Mater.* 12, 859–869
32 Steinem, C. *et al.* (2004) DNA hybridization-enhanced porous silicon corrosion: mechanistic investigations and prospect for optical interferometric biosensing. *Tetrahedron* 60, 11259–11267
33 Jane, A.O. *et al.* (2007) Porous silicon biosensor for the detection of autoimmune diseases. *Proceedings of SPIE - The International Society for Optical Engineering* 6799, 679908
34 Voelcker, N.H. *et al.* (2008) Catalyzed oxidative corrosion of porous silicon used as an optical transducer for ligand-receptor interactions. *ChemBioChem* 9, 1776–1786
35 Berger, M.G. *et al.* (1997) Dielectric filters made of PS: advanced performance by oxidation and new layer structures. *Thin Solid Films* 297, 237
36 Ilyas, S. *et al.* (2007) Porous silicon based narrow line-width rugate filters. *Opt. Mater.* 29, 619–622
37 Berger, M.G. *et al.* (1994) Porous superlattices: a new class of Si heterostructures. *J. Phys. D Appl. Phys.* 27, 1333–1336
38 Sailor, M.J. and Link, J.R. (2005) 'Smart dust': nanostructured devices in a grain of sand. *Chem. Commun. (Camb.)* (11), 1375–1383
39 Anderson, M.A. *et al.* (2003) Sensitivity of the optical properties of porous silicon layers to the refractive index of liquid in the pores. *Phys. Status Solidi, A Appl. Res.* 197, 528
40 Orosco, M. *et al.* (2006) Protein-coated porous-silicon photonic crystals for amplified optical detection of protease activity. *Adv. Mater.* 18, 1393
41 Kilian, K. *et al.* (2007) Peptide-modified optical filters for detecting protease activity. *ACS Nano* 1, 355–361
42 Schwartz, M.P. *et al.* (2006) The smart petri dish: a nanostructured photonic crystal for real-time monitoring of living cells. *Langmuir* 22, 7084–7090

43 Alvarez, S. *et al.* (2007) Using a porous silicon photonic crystal for bacterial cell-based biosensing. *Phys. Status Solidi, A Appl. Res.* 204, 1439–1443
44 Low, S.P. *et al.* (2006) Evaluation of mammalian cell adhesion on surface-modified porous silicon. *Biomaterials* 27, 4538–4546
45 Cunin, F. *et al.* (2002) Biomolecular screening with encoded porous-silicon photonic crystals. *Nat. Mater.* 1, 39–41
46 Canham, L.T. *et al.* (2000) Derivatized porous silicon mirrors: implantable optical components with slow resorbability. *Phys. Status Solidi, A Appl. Res.* 182, 521
47 Hardman, R. (2006) A toxicologic review of quantum dots: toxicity depends on physicochemical and environmental factors. *Environ. Health Perspect.* 114, 165–172
48 Chan, S. *et al.* (2001) Identification of gram negative bacteria using nanoscale silicon microcavities. *J. Am. Chem. Soc.* 123, 11797–11798
49 DeLouise, L.A. *et al.* (2005) Cross-correlation of optical microcavity biosensor response with immobilized enzyme activity. Insights into biosensor sensitivity. *Anal. Chem.* 77, 3222–3230
50 Karlsson, R. (2004) SPR for molecular interaction analysis: a review of emerging application areas. *J. Mol. Recognit.* 17, 151–161
51 Homola, J. *et al.* (2005) Multi-analyte surface plasmon resonance biosensing. *Methods* 37, 26
52 Ricci, F. *et al.* (2007) A review on novel developments and applications of immunosensors in food analysis. *Anal. Chim. Acta* 605, 111
53 Bonanno, L.M. and DeLouise, L.A. (2007) Whole blood optical sensor. *Biosens. Bioelectron.* 23, 444
54 Ouyang, H. *et al.* (2007) Label-free quantitative detection of protein using macroporous silicon photonic bandgap biosensors. *Anal. Chem.* 79, 1502–1506
55 Archer, M. *et al.* (2004) Macroporous silicon electrical sensor for DNA hybridization detection. *Biomed. Microdevices* 6, 203–211
56 Song, M.J. *et al.* (2007) Electrochemical biosensor array for liver diagnosis using silanization technique on nanoporous silicon electrode. *J. Biosci. Bioeng.* 103, 32
57 Wang, H. and Mu, S. (1999) Bioelectrochemical characteristics of cholesterol oxidase immobilised in a polyaniline film. *Sens. Actuators B Chem.* 56, 22–30
58 Setzu, S. *et al.* (2007) Porous silicon-based potentiometric biosensor for triglycerides. *Phys. Status Solidi, A Appl. Res.* 204, 1434
59 Xiao, C. *et al.* (2002) Structure characterization of porous silicon layers based on a theoretical analysis. *Langmuir* 18, 4165–4170
60 Vincent, G. (1994) Optical properties of porous silicon superlattices. *Appl. Phys. Lett.* 64, 2367
61 Pavesi, L. (1997) Random porous silicon multilayers: Application to distributed bragg reflectors and interferential fabry-perot filters. *Semicond. Sci. Technol.* 12, 570–575
62 Guillermain, E.E. *et al.* (2007) Bragg surface wave device based on porous silicon and its application for sensing. *Appl. Phys. Lett.* 90, 241116
63 Pavesi, L. (1997) Porous silicon dielectric multilayers and microcavities. *Rivista del Nuovo Cimento* 20, 1–76
64 Qian, M. *et al.* (2006) Structural tailoring of multilayer porous silicon for photonic crystal application. *J. Cryst. Growth* 292, 347–350